ACS APPLIED MATERIALS & INTERFACES

www.acsami.org

Research Article

Construction of a One-Dimensional Al-Rich ZSM-48 Zeolite with a Hollow Structure

Wen Liu, Junjie Li, Qiang Yu, Huihui Chen, Wenjuan Liu, Zhiqiang Yang, Xuebin Liu, Zhaochao Xu, Shutao Xu, Xiangxue Zhu,* and Xiujie Li*

Cite This: *ACS Appl. Mater. Interfaces* 2022, 14, 52025−52034

Read Online

ACCESS | Metrics & More | Article Recommendations | Supporting Information

ABSTRACT: Diffusion limitation and acid deficiency are two main challenges that the ZSM-48 zeolite faces in practical application. To date, there have been few effective strategies to solve both problems, simultaneously. Also, it is also a challenge to construct a hollow structure in a one-dimensional (1D) zeolite. Herein, an Al-rich ZSM-48 zeolite with a hollow structure is constructed through an alumination−recrystallization strategy, thereby solving the problems related to diffusion and acidity simultaneously. The hollowness and enrichment of aluminum can be controlled by judiciously matching the desilication and recrystallization. The silica to alumina ratio (SAR) of the ZSM-48 zeolite can be tuned from 130 to 45, which breaks the SAR limitation of conventional synthesis. On the basis of the different characterization results, the whole crystallization can be divided into two stages: rapid desilication−alumination and time-consuming recrystallization. In the selective desilication−recrystallization process, the preferential special distribution of the organic template leads to the formation of a hollow structure and the healing of mesopores at the outer shell, as evidenced by structured illumination microscopy images. Due to the enhancement in diffusion ability and acid density, the obtained hollow Al-rich ZSM-48 zeolite exhibits excellent catalytic stability and high *p*-xylene yield (∼26%) in the *m*-xylene isomerization reaction (WHSV = 18 h^{-1}), indicating its strong industrial application potential.

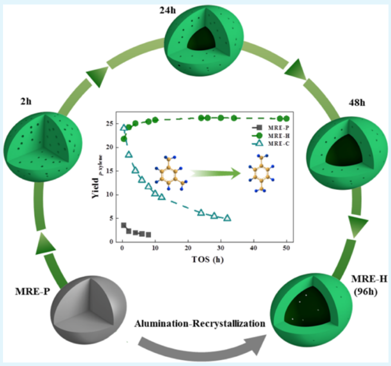

KEYWORDS: *ZSM-48 zeolite, diffusion limitation, acidity, hollow structure, m-xylene isomerization*

■ INTRODUCTION

Zeolites are crystalline materials with well-defined micropores and tailorable acidity, and they have been applied in a wide range of catalytic processes and other industrial processes.[1−3] As an important branch of zeolite materials, one-dimensional (1D) zeolites exhibit specific applications in the fields of isomerization.[4−7] Generally, 1D zeolites are easy to grow into rods or needles along the main channel direction, leading to severe diffusion limitation.[8−11] Moreover, such morphologies are harmful to human health as they easily penetrate into the respiratory system.[12] Hence, changing the growth trend of 1D zeolites and overcoming the problem of limited diffusion on the premise of good shape selectivity are of great importance.

The ZSM-48 zeolite (*MRE typology) is a type of high-silica zeolite with a 1D 10-membered ring (10-MR) channel (0.56 × 0.56 nm) along the [100] direction.[13] It exhibits excellent performance in alkane isomerization[14−16] and xylene isomerization.[9] Similar to that of other 1D zeolites, the typical morphology of the ZSM-48 zeolite is rods or needles, and its silica to alumina ratio (SAR) is generally higher than 200.[17,18] Thus, constrained diffusion along the main channel and low acid density restrict its application in specific reactions. Much efforts, including post-treatment and in situ synthesis methods, have been devoted to either improving diffusion or regulating acidity.[17−24] Liang and co-workers investigated the influence of alkaline treatment on the diffusion property of the ZSM-48 zeolite. After treatment, the ZSM-48 catalyst shows better performance in the hexadecane hydroisomerization reaction due to the introduction of new mesopore-accelerated molecule diffusion.[22,25] To enhance the diffusion property of the ZSM-48 zeolite, Che et al. applied a special surfactant with a polyphenyl structure to direct the synthesis of lamellar mesostructured ZSM-48 nanosheets.[21] We found that allyltrimethylammonium chloride is an effective organic structure directing agent (OSDA) to prepare the ZSM-48 zeolite with a low SAR.[17] However, there is still no effective strategy to solve both challenges related to diffusion limitation and low acid density, simultaneously.

m-Xylene isomerization aiming to transform low-valued *m*-xylene into a xylene mixture rich in *p*-xylene provides an important route for the industrial production of *p*-xylene. Up to now, ZSM-5, MOR, and EU-1 have been proved to be good isomerization catalyst candidates.[5,26] Unidimensional zeolites

Received: September 11, 2022
Accepted: October 31, 2022
Published: November 9, 2022

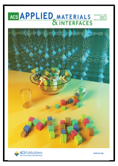

https://doi.org/10.1021/acsami.2c16346

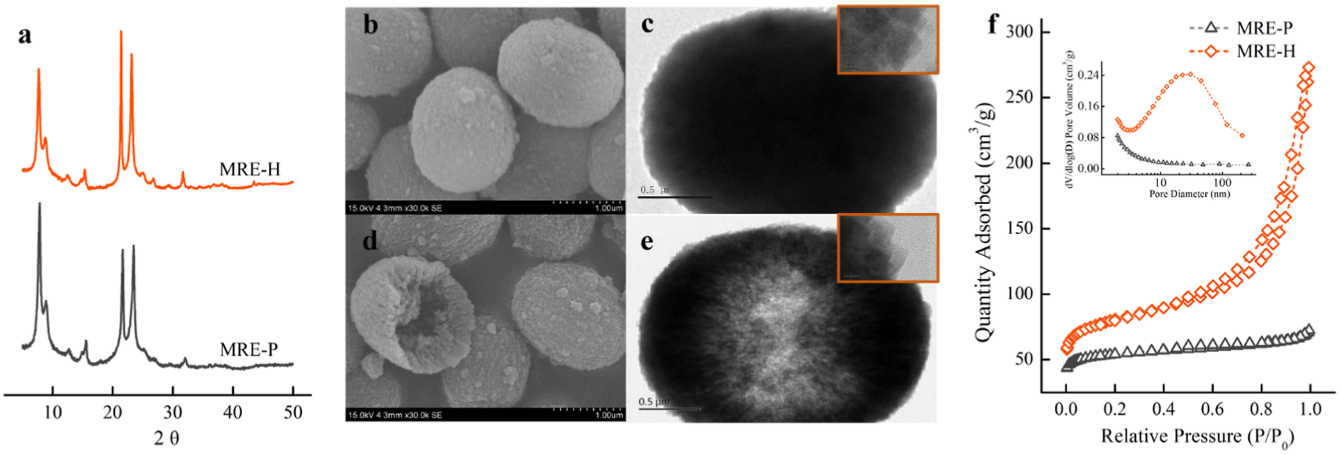

Figure 1. General information of MRE-P and MRE-H. (a) XRD patterns. SEM images [(b) MRE-P, (d) MRE-H] and low-magnification TEM images with a high-resolution TEM image in the inset [(c) MRE-P, (e) MRE-H]. (f) N_2 adsorption−desorption isotherm with the pore size distribution shown in the inset.

with 10-MR channels show high para-selectivity, but they easily are deactivated due to the diffusion restrictions.[5]

Hollow zeolites, whether hollow single crystal zeolites or agglomerated hollow zeolites, provide a suitable choice to alleviate the diffusion difficulty in a zeolite on the premise of maintaining zeolite crystallinity.[1,26] Several synthesis strategies, mainly including post-processing (selective desilication and desilication−recrystallization) and in situ synthesis strategies (soft template method and hard template method),[2,27] were developed to synthesize hollow zeolites with multidimensional pore structures, such as MFI,[28−31] Beta,[32,33] FAU,[34] and MWW.[35,36] However, few related reports about the preparation of hollow 1D zeolites were found. Herein, we developed an innovative alumination−recrystallization strategy to construct hollow Al-rich ZSM-48 zeolites, thereby solving the problems related to acidity and diffusion simultaneously. Key factors determining hollow structure construction and Al insertion were investigated and elucidated. After tracking the whole crystallization process, a reasonable recrystallization mechanism was proposed. The diffusion coefficient of hollow ZSM-48 is 7 times that of the parent sample when using *p*-xylene as the probe molecule. Moreover, the hollow Al-rich ZSM-48 zeolite exhibits remarkably enhanced stability and activity in the *m*-xylene isomerization reaction on the premise of its good *p*-xylene selectivity. *m*-Xylene conversion remains at 38.5% after 50 h on stream.

■ EXPERIMENTAL SECTION

Zeolite Synthesis. A hollow Al-rich ZSM-48 zeolite was synthesized by the alumination−recrystallization strategy as shown in Scheme S1. The obtained samples were named MRE-*x*-*y*, where *x* and *y* represent the NaOH concentration ($x \times 10^{-2}$ mol/L) and $Al_2(SO_4)_3$ ($y \times 10^{-2}$ mol/L) of initial solution, respectively; the specific synthesis parameters are shown in Table S1. Preferably, MRE-40-0.6 was also labeled MRE-H. To investigate the role of the OSDA, an etching experiment was performed, and the product was named MRE-D. In order to reveal the crystallization mechanism of the hollow Al-rich ZSM-48 zeolite, intermediates (including solids and filtrates) with different crystallization times were collected. The solid intermediates were named MRE-H-*t*h, where *t* represents the crystallization time (h). For comparison, the conventional ZSM-48 zeolite and ZSM-5 zeolite were synthesized by traditional hydrothermal methods, named MRE-C and ZC-5, respectively. The detailed experimental steps including the preparation of the parent zeolite were described in the Supporting Information.

Characterizations. Various characterization techniques including X-ray diffraction (XRD), N_2 adsorption−desorption analysis, X-ray fluorescence (XRF) analysis, X-ray photoelectron spectroscopy (XPS) analysis, inductively coupled plasma optical emission spectrometry analysis, scanning electron microscopy (SEM), transmission electron microscopy (TEM), high angle annular dark field scanning TEM (HAADF-STEM), Fourier-transform infrared (FT-IR), ^{27}Al signal pulse magic angle spinning nuclear magnetic resonance (MAS NMR), ^{27}Al multiple quantum (MQ)MAS NMR, ^{1}H MAS NMR, ammonia temperature programed desorption (NH_3-TPD), structure illumination microscopy (SIM), alkalinity analysis of solution, and the *p*-xylene adsorption test were adopted to measure the physical and chemical properties of zeolite samples. The detailed measurement information was described in the Supporting Information.

Catalytic Evaluation. *m*-Xylene isomerization was chosen as the probe reaction to evaluate the catalytic performance of catalysts. The detailed measuring processes are described in the Supporting Information.

■ RESULTS AND DISCUSSION

Physicochemical Properties of the Hollow Al-Rich ZSM-48 Zeolite. Figure 1 lists the general information of the parent ZSM-48 (MRE-P) and hollow Al-rich ZSM-48 zeolite (MRE-H). MRE-P and MRE-H show typical diffraction peaks assigned to the *MRE phase according to the XRD patterns (Figure 1a).[13] MRE-P is a monodispersed ellipsoidal dense crystal with a particle size of 1.5 μm × 2 μm (Figure 1b,c). After the alumination−recrystallization process, an obvious hollow structure is formed as shown in Figure 1d,e. Clear lattice fringes and the large micropore volume (V_{micro}, 0.072 cm^3/g) guarantee its high crystallinity. The N_2 uptake isotherm rises rapidly at high relative pressure (Figure 1f), and a typical H4 hysteresis loop is observed for MRE-H implying its hierarchical property (Table S2). Moreover, a mesopore distribution at 3−30 nm is observed in the pore-size distribution curves derived by Hg intrusion, which proves the pore connectivity of the hollow structure (Figure S1).[37] Also, the distribution of macropores at about 750 nm echoes the hollow size observed from the TEM image. At the same time, its SAR decreases from 227 to 51 (Table S1).

Parametric Study on the Hollow Al-Rich ZSM-48 Zeolite. A parametric study reveals that desilication and recrystallization are the key factors determining the synthesis

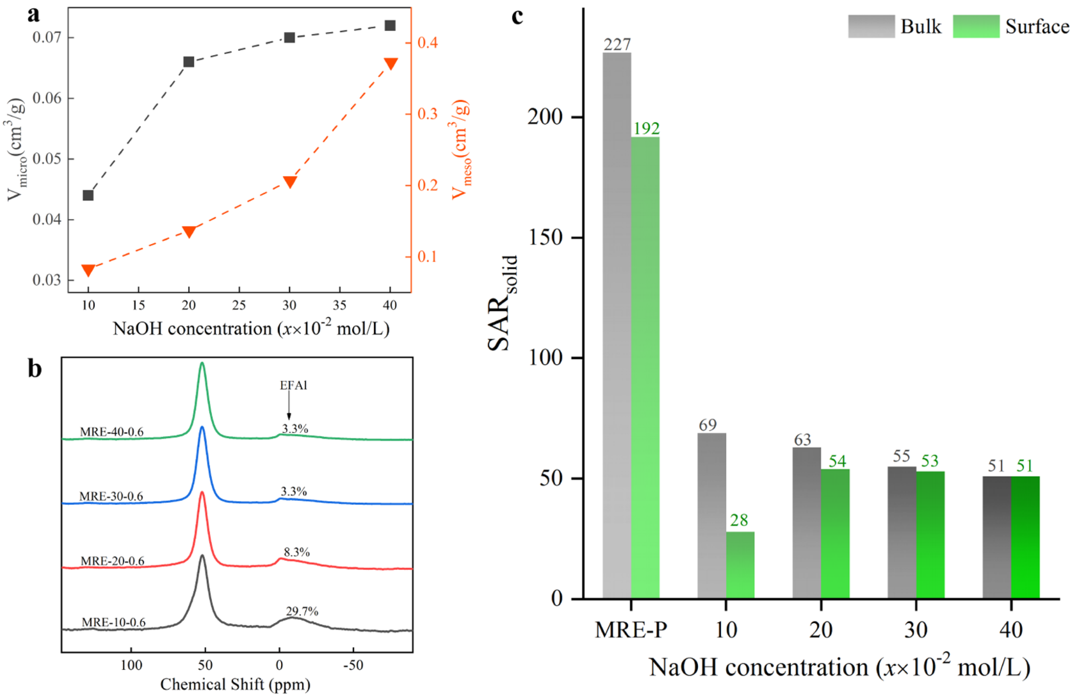

Figure 2. (a) Diagram of micropore and mesoporous volume of the solid product as a function of initial solution alkalinity; (b) ^{27}Al MAS NMR spectra of MRE-*x*-0.6 samples; and (c) bulk and surface SAR of MRE-*x*-0.6 samples (bulk SAR determined by XRF and surface SAR determined by XPS).

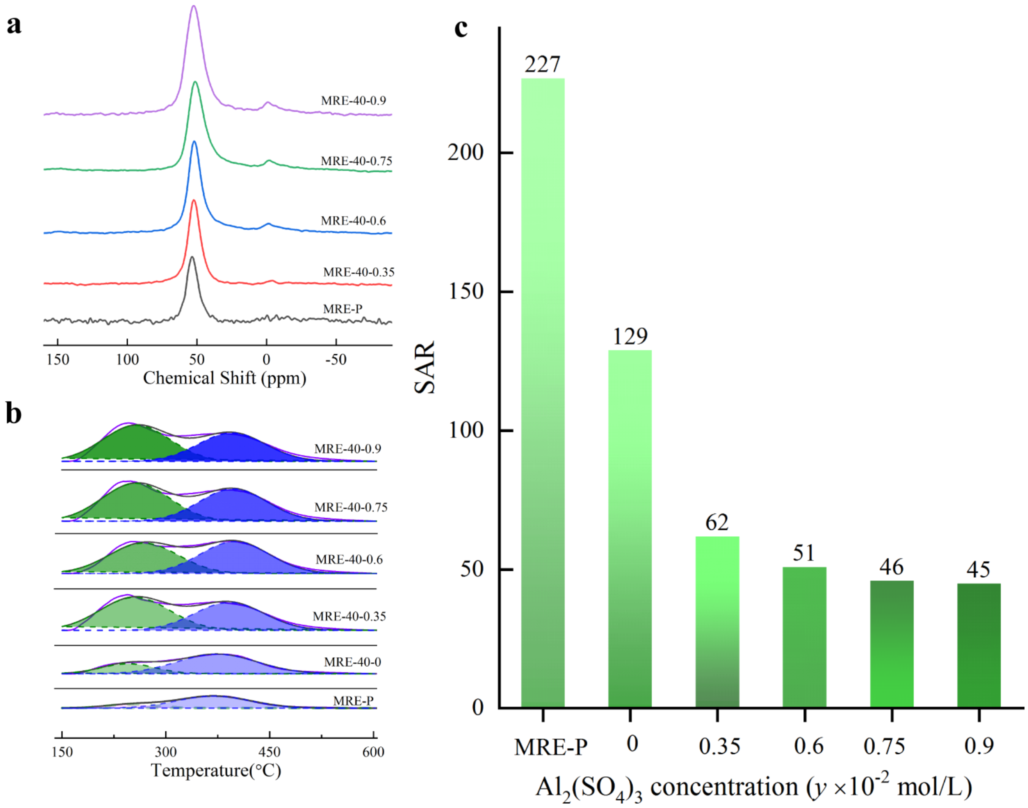

Figure 3. (a) ^{27}Al MAS NMR spectra, (b) NH_3-TPD profiles, and (c) SAR determined by XRF of MRE-P and MRE-40-*y* samples.

of the hollow Al-rich ZSM-48 zeolite. Desilication is closely related to the alkalinity of the system (NaOH concentration). As shown in the XRD patterns (Figure S2) and TEM images (Figure S3), a suitable alkalinity (20−40 × 10^{-2} mol/L) is required for preparing hollow Al-rich ZSM-48 zeolites. The XRD line intensities of recrystallized products are obviously weaker than those of MRE-P, which may be attributed to the changes of the SAR and introduction of mesopores.[38] The hollowness and the N_2 adsorption volume at high P/P_0 (Figure S4) increase with the alkalinity from 0.2 to 0.4 mol/L, which

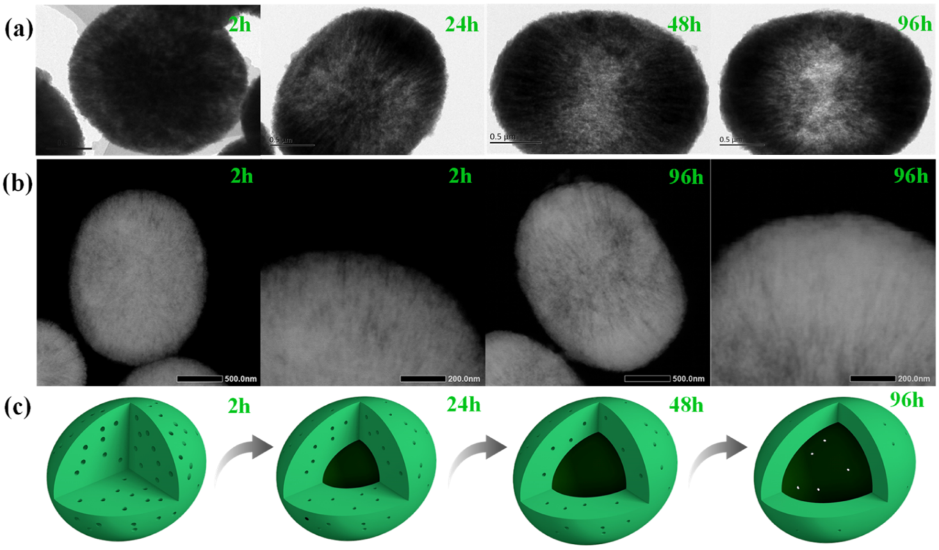

Figure 4. (a) TEM images and (b) HAADF-STEM images of MRE-H with different crystallization times. (c) Schematic of the structural evolution of MRE-H.

suggests that a higher alkalinity results into a much larger mesopore volume (V_{meso}) combined with detailed textural data in Table S2. This indicates that the formation of a hollow structure is due to from alkali etching. Generally, the introduction of mesopores into zeolites through desilication will weaken the integrity of the microporous structure, resulting in an obvious decrease in V_{micro}.[22,25] However, the V_{micro} and V_{meso} increase simultaneously upon alkalinity (Figure 2a), indicating that the post-treatment process includes not only desilication etching but also recrystallization. The symmetric tetra-coordinated Al signal and the negligible hexa-coordinated Al signal attributed to extra-framework Al shown in the ^{27}Al MAS NMR spectrum (Figure 2b) also support the recrystallization in this process. Moreover, the alkalinity of the system influences the bulk SAR of the samples. As shown in Figure 2C, high alkalinity of the initial solution leads to a low bulk SAR due to the severe desilication. Under high alkalinity (>0.45 mol/L), the EUO hetero-phase appears in the XRD patterns (Figure S2), and rectangular-like EUO crystals can be observed in SEM images (Figure S5). This suggests that a high alkalinity is prone to induce EUO impurity in an Al-rich environment, which is in accordance with the findings of Giordano et al.[39] Under low alkalinity (<0.1 mol/L), recrystallization is suppressed. Obvious increase in extra-framework Al (Figure 2b) and a low V_{micro} (0.044 cm^3/g) for MRE-10-0.6 can be observed (Table S2). Moreover, its surface SAR is lower than that of the bulk (Figure 2c) indicating that the surface enrichment of Al species is due to the lack of mesoporous channels for diffusion, further leading to the partial blockage of micropores. In summary, suitable alkalinity plays important roles during the recrystallization process. One is creating the mesopores and hollow structure through desilication; the other is to promote Al species into the internal crystal through the mesopore and coordinate them into the framework with the assistance of the OSDA (HM^{2+} ions). The combination of desilication and Al insertion promotes the formation of aluminum enrichment of the ZSM-48 zeolite framework.

A suitable Al species concentration is also required for the formation of the hollow structure and Al-rich framework. XRD patterns in Figure S6 show that all samples exhibit typical *MRE diffraction peaks, and no impurity is formed with the variation of the Al concentration. SEM and TEM images (Figure S7) show that large numbers of fragments are formed when the Al species are absent, while the fragments disappear, and the hollow ZSM-48 zeolite with the regular shell structure is formed accompanied by the introduction of Al species. Moreover, the size of the hollow structure gradually shrinks upon Al species concentration. This is also supported by the gradual shrinkage of V_{meso} (Table S2) with the increase in the Al species concentration. ^{27}Al MAS NMR spectra exhibit that all the recrystallized samples show a main tetra-coordinated Al signal and a negligible hexa-coordinated Al signal, and the intensities of tetra-coordinated Al are significantly enhanced than those of MRE-P (Figure 3a), which indicates that supplementary Al species are incorporated into the framework. The increase in acid density (Figure 3b, Table S3) verifies the coordination of Al species into the framework. It should be noted here that the introduction of Al species shows little effect on the pH value of the system (Figure S8). Therefore, it can be concluded that Al species not only play a role in protecting the zeolite framework from serious damage but also enrich the framework Al density of the ZSM-48 zeolite through recrystallization coordination into the framework. In addition, the SAR of the product decreases gradually as shown in Figure 3c with the increasing concentration of Al species. That is, the SAR of the ZSM-48 zeolite can be regulated in a large range (135−45) by simply changing the concentration of Al species in the initial solution.

Crystallization Mechanism of the Hollow Al-Rich ZSM-48 Zeolite. The formation mechanism of the hollow Al-rich ZSM-48 zeolite was investigated using MRE-H (MRE-40-0.6) as a candidate. In the time-resolved XRD patterns (Figure S9), diffraction peaks assigned to the *MRE phase can be observed throughout the whole process, indicating that the main framework is always preserved. TEM images provide direct evidence for the evolution of the zeolite structure. After crystallization for 2 h, some randomly distributed intracrystalline mesopores are formed (Figure 4a), which is well supported by an increase in V_{meso} from 0.04 to 0.43 cm^3/g (Table S4). The etching of the inner part of the zeolite crystal becomes increasingly visible with prolonged heating, and a

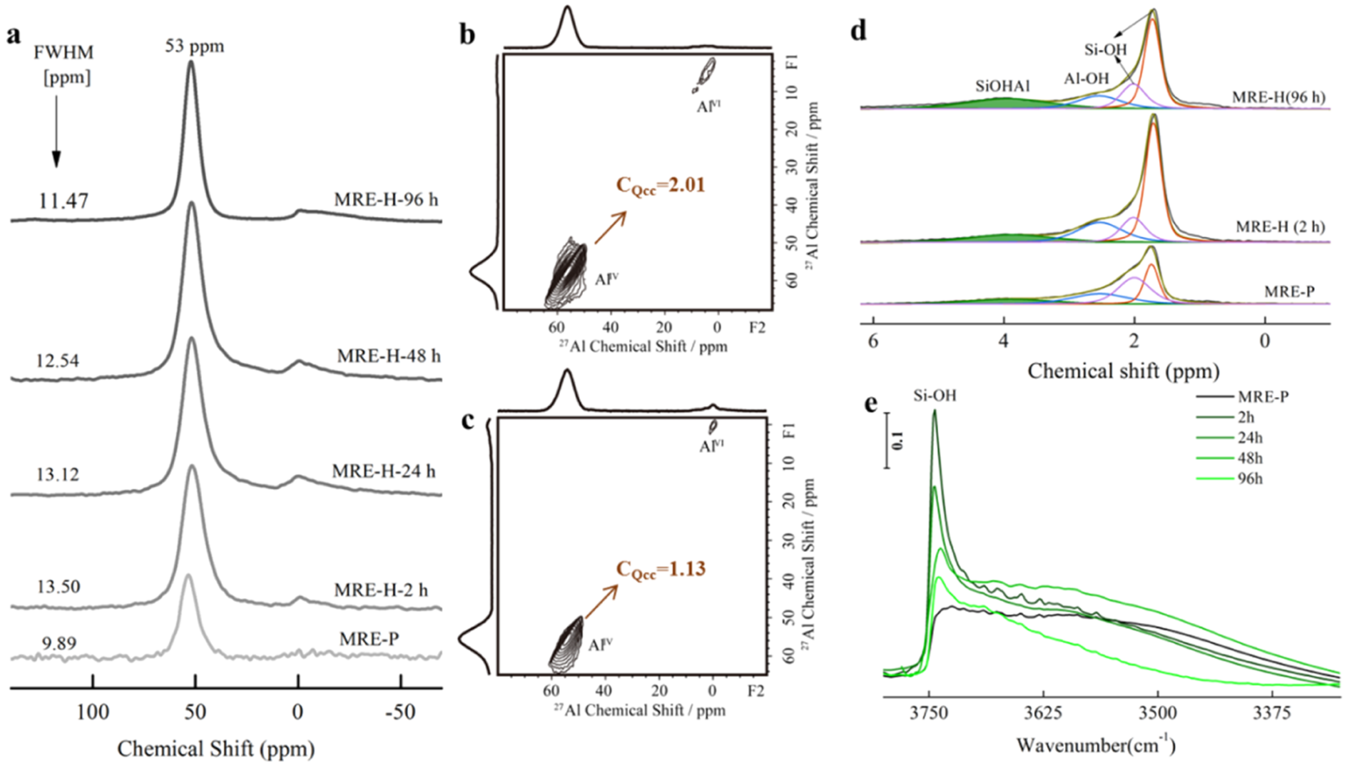

Figure 5. (a) ^{27}Al MAS NMR spectra of MRE-P and MRE-H with different crystallization times; ^{27}Al MQMAS NMR spectra of (b) MRE-P and (c) MRE-H; (d) ^{1}H MAS NMR spectra; and (e) FT-IR spectra for MRE-P and MRE-H with different crystallization times.

hollow structure is formed gradually. Meanwhile, the edge of the crystal becomes clearer and smoother after 96 h of heating, indicating that the outer shell of the zeolite crystal is gradually repaired (Figure 4b). An increase in V_{micro} and a decrease in V_{meso} also support the recrystallization at the outer shell (Figure S10 and Table S4). Upon further extending the crystallization time to 120 h, the texture properties of the products change little, indicating the end of recrystallization at 96 h. The SEM images (Figure S11) show that the particle size changes slightly during the whole process. Also, no new layers are found in TEM images. Thus, it can be tentatively concluded that the recrystallization of the ZSM-48 zeolite is not the formation of new crystalline layers as previously reported for the MFI zeolite[30,31] but the repairing of the defects on the crystal shell. The increase in the average pore diameter and the large reduction of small-size mesopores (Table S4, Figure S10) also indicate that the healing of mesopores evolves with crystallization. On the basis of the above-mentioned discussion, an idealized schematic for the structural evolution of MRE-H is proposed and listed in Figure 4c.

To verify the coordination state of Al species, ^{27}Al (MQ)MAS NMR, ^{1}H MAS NMR, and FT-IR spectra were recorded. After heating for 2 h, an enhancement of the signal at 53 ppm (assigned to tetra-coordinated Al) compared with that of MRE-P can be clearly observed in the time-resolved ^{27}Al MAS NMR spectra (Figure 5a), which suggests that the supplementary Al species combined with the active Si species (Si−OH) to form the Si−O−Al structure. The gradual narrowing of the full width at half-maximum (FWHM) of the tetra-coordinated Al signal with time indicates that the Al species are inserted into the framework to form a more ordered Si−O−Al structure. In the ^{27}Al MQMAS NMR spectra, the quaternary coupling factor (C_{Qcc}) of tetrahedral Al at 96 h is smaller than that at 2 h, which also confirms the good coordination symmetry of the framework Al species (Figure 5b,c). To further verify the coordination of Al species into the framework, the evolution of product acidity was investigated. As shown in ^{1}H MAS NMR spectra, the resonance signal at 3.9 ppm, which is associated with the Brönsted acid sites, increases clearly with time (Figure 5d, Table S3). The desorption peak assigned to the strong acid site in NH_3-TPD profiles also shows the similar changing trend (Figure S12, Table S3). All these characterization results provide direct evidence for the incorporation of Al species into the framework.

The information of silanol groups with different crystallization times is traced using FT-IR as shown in Figure 5e. After crystallization for 2 h, the infrared signal at 3740 cm^{-1} ascribed to the free silanol group increases significantly, indicating that extensive defect sites are formed due to desilication at the initial stage. This could further be verified in the ^{1}H MAS NMR spectra. As shown in Figure 5d, the peak intensity assigned to Si−OH for MRE-H-2h is also highly enhanced. After 2 h, the number of the silanol groups gradually decreases upon the crystallization time, indicating that the healing of defect sites happens. Combined with ^{27}Al MAS NMR results, it could be deduced that the supplemented Al species incorporated into the framework through the condensation between hydroxyls. After 96 h, the number of hydroxyl groups is still larger than that of the parent sample due to the formation of the hollow structure.

Based on the above-mentioned discussion, it can be concluded that the hollow structure is derived from the etching of the inner crystal and the recrystallization of the outer shell by healing defects/mesopores. However, the working mechanism remains elusive. In order to figure it out,

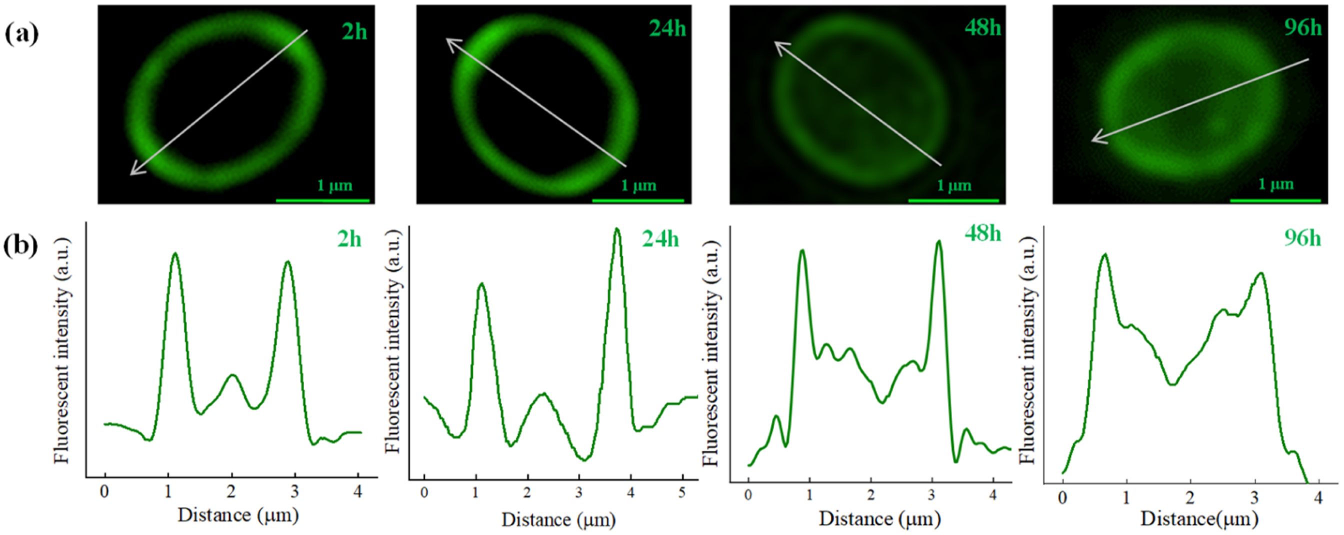

Figure 6. (a) SIM images and (b) corresponding fluorescence intensity distribution curves of MRE-H with different crystallization times.

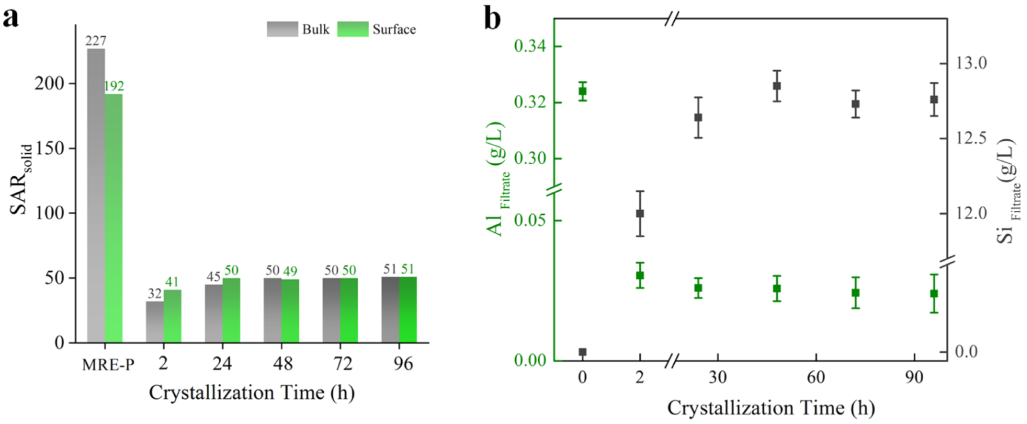

Figure 7. (a) Solid bulk and surface SAR of MRE-P and MRE-H with different crystallization times. (b) Si and Al content of the filtrate with different crystallization times.

SIM was applied to track the evolution of the spatial distribution of OSDA molecules at the single zeolite crystal level during crystallization. Weckhuysen et al. found that the decomposition of the template molecules in zeolite crystals affords the formation of fluorescent intermediates which can be monitored by fluorescence microscopy.[40] As shown in Figure 6a,b, a clear fluorescence signal is observed around the outer shell of the ellipsoidal crystal at the initial stage of crystallization. With the extension of crystallization time, the fluorescence signal inside the crystal gradually intensifies, but obvious signal attenuation can still be observed from the outer shell to the inside of the crystal. This indicates that the OSDA (HM^{2+} ions) preferentially adsorbs on the external surface and slowly migrates into the interior part due to diffusion limitation. Because of the shell protection from the OSDAs, etching is dominant in the internal crystals, directly leading to the formation of a hollow structure. Moreover, with the assistance of OSDAs, recrystallization and defect healing happen preferentially in the external crystal, resulting in the formation of Al-rich shell crystals with high crystallinity. In order to better understand the important role of the OSDA, an etching experiment was performed by dispersing the parent zeolite into an initial solution in the absence of the OSDA followed by dynamic treatment for 96 h at 160 °C. As shown in Figure S13, the framework of the ZSM-48 zeolite is completely dismembered and transformed into lamellar magadiite. This well supports the important role of the OSDA in protecting the zeolite framework and promoting recrystallization. To the best of our knowledge, this is the first time that experimental data are provided to support the formation mechanism of hollow zeolites through a post-treatment strategy.

The elemental analysis of the solids and filtrates was investigated to better understand the recrystallization process in terms of solid−liquid mass transfer. During the initial 2 h, the bulk and surface SAR decreases significantly; at the same time, a large amount of Si species is extracted from the framework, and most of the Al species are transferred into the solids (Figure 7a,b). It should be noted here that no surface enrichment of Al species is observed. These results suggest that desilication mainly occurs during the initial 2 h, yielding abundant mesopores beneficial for the migration anchorage of Al species,[41] which is also the essential driving force of extensive defects in the initial stage. This conclusion is also supported by a drastic decrease in the filtrate pH value due to alkali consumption in desilication (Figure S14). Subsequently, a dynamic balance between the internal etching and external recrystallization is established on the basis of the little change

https://doi.org/10.1021/acsami.2c16346
ACS Appl. Mater. Interfaces 2022, 14, 52025−52034

Scheme 1. Proposed Evolution Mechanism for the Recrystallization Process

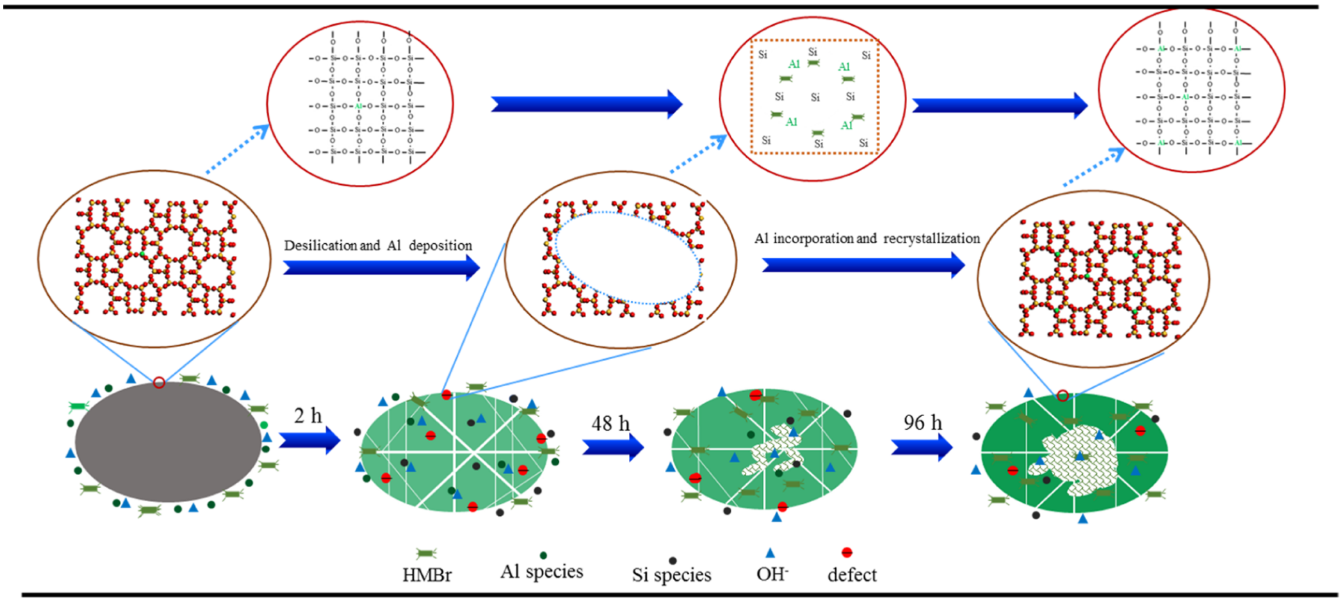

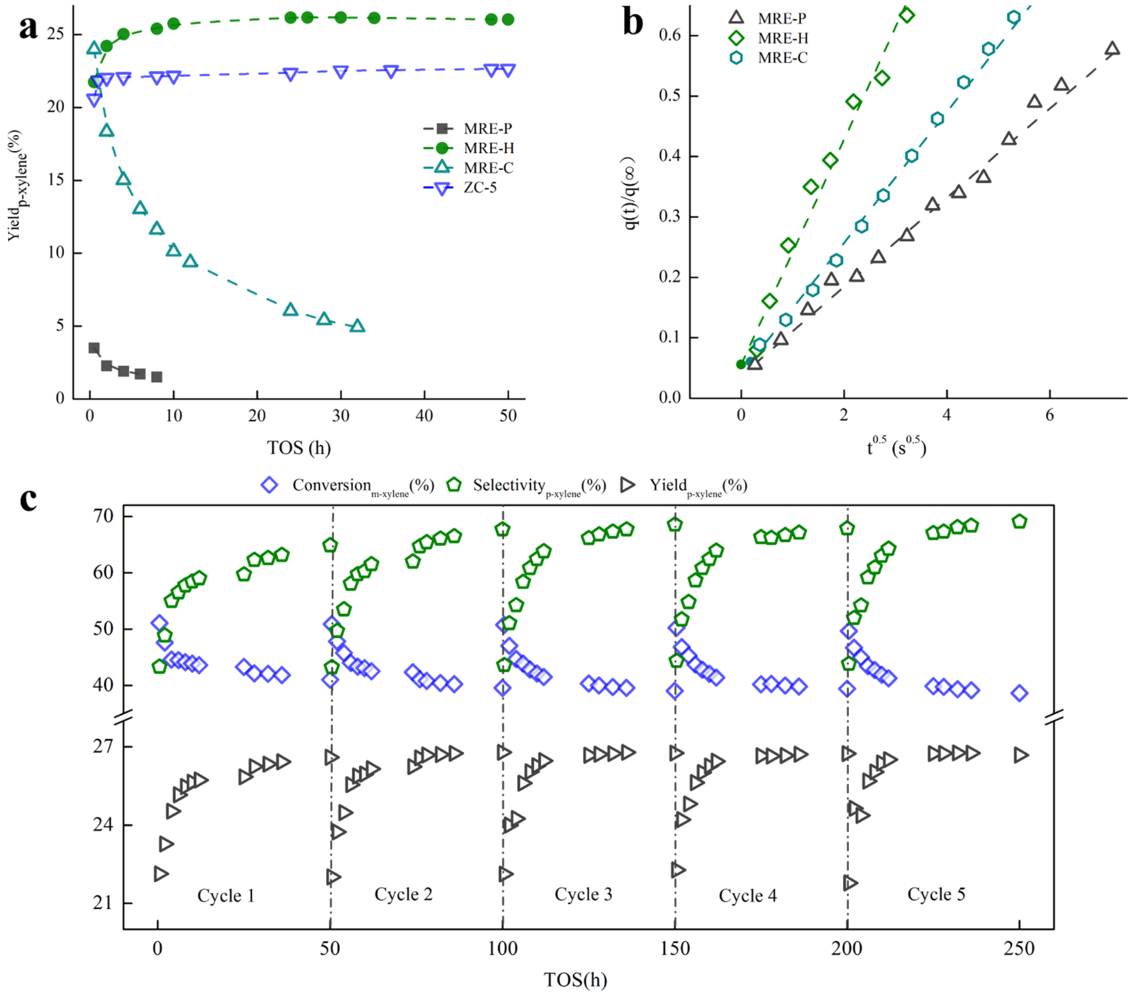

Figure 8. (a) *p*-Xylene yield of various catalysts in *m*-xylene isomerization as a function of time on the stream; (b) *p*-xylene uptake kinetics curves; and (c) recyclability of the MRE-H catalyst.

of the solid SAR and the Si (or Al) content in the filtrate. It can be concluded that the recrystallization process includes not only the insertion of supplemented Al species but also the coordination of dissolved silicon species into the zeolite framework with the assistance of the OSDA.

From the above-mentioned experimental results, an ingenious recrystallization mechanism is proposed (Scheme 1). Briefly, the alumination−recrystallization process includes two stages: rapid desilication accompanied by Al immigration and time-consuming recrystallization accompanied by Al incorporation into the framework. In stage I, desilication of the parent zeolite dominates, and abundant mesopores are formed. Meanwhile, the deposited Al species diffuse into the inner part of crystals through mesopores. In stage II, the Al species are gradually incorporated into the framework by the healing of the mesopores or defects in the outer shell with the assistance of the OSDA. The formation of the hollow structure is mainly attributed to the spatial mismatch of dissolution and recrystallization between the internal crystal and outer shell, which is essentially driven by the uneven spatial distribution of OSDA molecules.

Evaluation of Catalytic Performance. *m*-Xylene isomerization was chosen as a probe reaction to evaluate the catalytic performance of ZSM-48 samples. In order to highlight the catalytic advantages of the obtained hollow Al-rich ZSM-48 zeolite, the conventional ZSM-48 zeolite (labeled MRE-C) and typical isomerization catalyst ZSM-5 zeolite (labeled ZC-5) were used as references. Their detailed properties are listed in Figures S15 and S16 and Table S5.

As shown in Figure S17a, the *m*-xylene conversion on ZC-5 remains at 50% after 50 h on stream, and the *p*-xylene selectivity is around 45% (Figure S17b), which is consistent with previous reports.[5] Three ZSM-48 catalysts show higher *p*-xylene selectivity compared with the ZC-5 catalyst (Figure S17c). In particular, MRE-H shows the highest *p*-xylene yield (>26%) among four catalysts (Figure 8a), and the ratio of *p*-xylene to *o*-xylene is almost twice that of the ZC-5 catalyst (Figure S17c). The initial ratio of isomerization to disproportionation reaction (*i/d*) is similar for MRE-H and ZC-5. After 24 h, the i/d ratio of MRE-H is much higher than that of ZC-5 (73.0 vs 8) (Figure S17d). This suggests that the ZSM-48 zeolite could inhibit the disproportionation side reactions and show better shape selectivity than the ZSM-5 zeolite due to its unique 1D pore system.

For three ZSM-48 samples, MRE-P shows the lowest *p*-xylene yield due to its low acid density and large crystal size. High initial *p*-xylene yield is observed on MRE-C. However, it deactivates quickly, and the *p*-xylene yield is lowered to 8% after 30 h on stream. In the case of MRE-H, *m*-xylene conversion remains at 38.5% after 50 h on stream, showing its excellent catalytic stability. The different stability of the three ZSM-48 catalysts is rooted in the difference of their diffusion properties. To confirm this conclusion, the adsorption experiment was carried out using *p*-xylene as the probe molecule. As shown in Figure S18, MRE-H shows the maximum static uptake amount of *p*-xylene due to its hierarchy of the pore structure and the introduction of the hollow structure. In the case of the adsorption rate (Figure 8b), the diffusion time constant (D_{eff}/L^2) of MRE-H is over 7 times that of MRE-P ($3.07 \times 10^{-2}\ \mathrm{s}^{-1}$ vs $4.24 \times 10^{-3}\ \mathrm{s}^{-1}$) and over 3 times that of MRE-C ($3.07 \times 10^{-2}\ \mathrm{s}^{-1}$ vs $9.50 \times 10^{-3}\ \mathrm{s}^{-1}$). The TG results of the spent catalysts (Figure S19) also support this conclusion. The coke content (200−820 °C) of MRE-C is over 2.6 times that of MRE-H (8.52% vs 3.19%), indicating that the hollow ZSM-48 zeolite has better carbon deposition resistance. In order to test the regeneration performance of MRE-H, the cyclic catalysis experiment was performed. As shown in Figure 8c, its performance remains as good as that of a fresh catalyst after five cycles, indicating its strong potential for industrial applications.

■ CONCLUSIONS

An innovative preparation approach for an Al-rich ZSM-48 zeolite with a hollow structure was developed for the first time. The diffusion capacity is improved by over 6 times, and the SAR can be regulated between 130 and 45 by judiciously matching the desilication and recrystallization rate. The evolution of the recrystallization process was tracked through different characterization tools. In general, the whole process can be divided into two stages: rapid desilication along with aluminum deposition−redispersion and time-consuming recrystallization. From the ingenious implementation of SIM, it is confirmed that the selective adsorption of the OSDA on the external crystal directly leads to the spatial mismatch of dissolution and recrystallization between the internal crystal and outer shell, further resulting in the formation of a hollow structure. This provides intuitive experimental support for the popular hypothesis of constructing hollow structures through post-treatment. Benefited from the enhancement in diffusion property and acid density, the hollow Al-rich ZSM-48 zeolite exhibits better stability and activity compared with the parent sample in *m*-xylene isomerization. Also, higher *p*-xylene yield (~26%) than that of the traditional ZSM-5 catalyst is obtained. This work provides references for improving the diffusivity and acidity of 1D zeolites by including a strategy and characterization.

■ ASSOCIATED CONTENT

Supporting Information

The Supporting Information is available free of charge at https://pubs.acs.org/doi/10.1021/acsami.2c16346.

Experimental section, supplementary figures, and supplementary tables (PDF)

■ AUTHOR INFORMATION

Corresponding Authors

Xiangxue Zhu − *Dalian National Laboratory for Clean Energy, Dalian Institute of Chemical Physics, Chinese Academy of Sciences, Dalian 116023, China;* orcid.org/0000-0002-0658-9173; Email: zhuxx@dicp.ac.cn

Xiujie Li − *Dalian National Laboratory for Clean Energy, Dalian Institute of Chemical Physics, Chinese Academy of Sciences, Dalian 116023, China;* orcid.org/0000-0002-2649-4673; Email: xiujieli@dicp.ac.cn

Authors

Wen Liu − *Dalian National Laboratory for Clean Energy, Dalian Institute of Chemical Physics, Chinese Academy of Sciences, Dalian 116023, China; University of Chinese Academy of Sciences, Beijing 100049, China*

Junjie Li − *Dalian National Laboratory for Clean Energy, Dalian Institute of Chemical Physics, Chinese Academy of Sciences, Dalian 116023, China*

Qiang Yu − *Dalian National Laboratory for Clean Energy, Dalian Institute of Chemical Physics, Chinese Academy of Sciences, Dalian 116023, China; University of Chinese Academy of Sciences, Beijing 100049, China*

Huihui Chen − *Dalian National Laboratory for Clean Energy, Dalian Institute of Chemical Physics, Chinese Academy of Sciences, Dalian 116023, China; University of Chinese Academy of Sciences, Beijing 100049, China*

Wenjuan Liu − *Dalian National Laboratory for Clean Energy, Dalian Institute of Chemical Physics, Chinese Academy of Sciences, Dalian 116023, China*

Zhiqiang Yang − *Applied Sciences, BP Innovation & Engineering, Energy Innovation Laboratory, BP Office (Dalian Institute of Chemical Physics), Dalian 116023, China*

Xuebin Liu − *Applied Sciences, BP Innovation & Engineering, Energy Innovation Laboratory, BP Office (Dalian Institute of Chemical Physics), Dalian 116023, China*

Zhaochao Xu − *Dalian National Laboratory for Clean Energy, Dalian Institute of Chemical Physics, Chinese Academy of Sciences, Dalian 116023, China;* orcid.org/0000-0002-2491-8938

Shutao Xu − *Dalian National Laboratory for Clean Energy, Dalian Institute of Chemical Physics, Chinese Academy of Sciences, Dalian 116023, China;* orcid.org/0000-0003-4722-8371

Complete contact information is available at:
https://pubs.acs.org/10.1021/acsami.2c16346

Author Contributions

The manuscript was written through contributions of all authors. All authors have given approval to the final version of the manuscript.

Notes

The authors declare no competing financial interest.

ACKNOWLEDGMENTS

This project has received funding from the National Natural Science Foundation of China (nos. 22172162, U20A20120), BP Energy Innovation Laboratory (EIL-045), Dalian Innovation Team in Key Areas (2020RT06), STS Network Initiative (KFJ-STS-QYZD-2021-17-001/002), and the Strategic Priority Research Program of the CAS (XDA 21000000).

REFERENCES

(1) Li, S.; Li, J.; Dong, M.; Fan, S.; Zhao, T.; Wang, J.; Fan, W. Strategies to Control Zeolite Particle Morphology. *Chem. Soc. Rev.* **2019**, *48*, 885−907.

(2) Chen, L. H.; Sun, M. H.; Wang, Z.; Yang, W.; Xie, Z.; Su, B. L. Hierarchically Structured Zeolites: From Design to Application. *Chem. Rev.* **2020**, *120*, 11194−11294.

(3) Zhang, M.; Long, H.; Fan, D.; Wang, L.; Wang, Q.; Chen, Y.; Sun, L.; Qi, C. Synthesis of ZSM-48 Zeolites and Their Catalytic Performance: A Review. *Catal. Sci. Technol.* **2022**, *12*, 5097−5109.

(4) Noh, G.; Zones, S. I.; Iglesia, E. Isomer Sieving and The Selective Formation of Terminal Methyl Isomers in Reactions of Linear Alkanes on One-Dimensional Zeolites. *J. Catal.* **2019**, *377*, 255−270.

(5) Min, H.-K.; Cha, S. H.; Hong, S. B. Mechanistic Insights into the Zeolite-Catalyzed Isomerization and Disproportionation ofm-Xylene. *ACS Catal.* **2012**, *2*, 971−981.

(6) Wei, C.; Zhang, G.; Zhao, L.; Gao, J.; Xu, C. Effect of metal-acid balance and textual modifications on hydroisomerization catalysts for n-alkanes with different chain length: A mini-review. *Fuel* **2022**, *315*, 122809.

(7) Meng, J.; Cui, T.; Bai, D.; Li, C.; Chen, X.; Liang, C. Excellent Catalytic Performance over Hierarchical ZSM-48 Zeolite: Cooperative Effects of Enhanced Mesoporosity and Highly-Accessible Acidity. *Fuel* **2022**, *324*, 124589.

(8) Okamoto, M.; Nishimura, Y.; Takahashi, M.; Chen, W.-H. Synthesis of Short, Needle-Shaped Crystals of TON-Type Zeolite by Addition of Inhibitors of Crystal Growth along the [001] Direction. *Cryst. Growth Des.* **2018**, *18*, 6573−6580.

(9) Liu, W.; Li, J.; Liu, Z.; Yang, Z.; Liu, X.; Tan, X.; Xu, L.; Li, X.; Zhu, X. Direct Preparation of *MRE Zeolites with Ultralarge Mesoporosity: Strategy and Working Mechanism. *Appl. Mater. Interfaces* **2021**, *13*, 31756−31765.

(10) Molino, A.; Holzinger, J.; Łukaszuk, K. A.; Rojo-Gama, D.; Gunnæs, A. E.; Skibsted, J.; Lundegaard, L. F.; Svelle, S.; Beato, P.; Bordiga, S.; Lillerud, K. P. Synthesis of ZSM-23 (MTT) Zeolites with Different Crystal Morphology and Intergrowths: Effects on the Catalytic Performance in the Conversion of Methanol to Hydrocarbons. *Catal. Sci. Technol.* **2019**, *9*, 6782−6792.

(11) Alaithan, Z. A.; Harrison, N.; Sastre, G. Diffusivity of Propylene in One-Dimensional Medium-Pore Zeolites. *J. Phys. Chem. C* **2021**, *125*, 19200−19208.

(12) Ma, Y.; Tang, X.; Hu, J.; Ma, Y.; Chen, W.; Liu, Z.; Han, S.; Xu, C.; Wu, Q.; Zheng, A.; Zhu, L.; Meng, X.; Xiao, F. S. Design of a Small Organic Template for the Synthesis of Self-Pillared Pentasil Zeolite Nanosheets. *J. Am. Chem. Soc.* **2022**, *144*, 6270−6277.

(13) Lobo, R. F.; van Koningsveld, H. New Description of the Disorder in Zeolite ZSM-48. *J. Am. Chem. Soc.* **2002**, *124*, 13222−13230.

(14) Kim, J.; Han, S. W.; Kim, J.-C.; Ryoo, R. Supporting Nickel To Replace Platinum on Zeolite Nanosponges for Catalytic Hydroisomerization of *n*-Dodecane. *ACS Catal.* **2018**, *8*, 10545−10554.

(15) Zhang, M.; Chen, Y.; Wang, L.; Zhang, Q.; Tsang, C.-W.; Liang, C. Shape Selectivity in Hydroisomerization of Hexadecane over Pt Supported on 10-Ring Zeolites: ZSM-22, ZSM-23, ZSM-35, and ZSM-48. *Ind. Eng. Chem. Res.* **2016**, *55*, 6069−6078.

(16) Zhang, M.; Li, C.; Chen, Y.; Tsang, C.-W.; Zhang, Q.; Liang, C. Hydroisomerization of Hexadecane over Platinum Supported on EU-1/ZSM-48 Intergrowth Zeolite Catalysts. *Catal. Sci. Technol.* **2016**, *6*, 8016−8023.

(17) Zhai, M.; Ding, H.; Zeng, S.; Jiang, J.; Xu, S.; Li, X.; Zhu, K.; Zhou, X. Aluminous ZSM-48 Zeolite Synthesis Using a Hydroisomerization Intermediate Mimicking Allyltrimethylammonium Chloride as a Structure-Directing Agent. *Ind. Eng. Chem. Res.* **2020**, *59*, 11139−11148.

(18) Meng, J.; Li, C.; Chen, X.; Song, C.; Liang, C. Seed-Assisted Synthesis of ZSM-48 Zeolite with Low SiO_2/Al_2O_3 Ratio for *n*-Hexadecane Hydroisomerization. *Microporous Mesoporous Mater.* **2020**, *309*, 110565.

(19) Liu, X. L.; Wang, X. J.; Wang, Y.; Gong, Y. J.; Dou, T. Synthesis and Characterization of Hierarchical ZSM-48 Zeolite. *Adv. Mater. Res.* **2012**, *503*−*504*, 756−759.

(20) Astafan, A.; Benghalem, M. A.; Michelin, L.; Rigolet, S.; Patarin, J.; Pinard, L.; Daou, T. J. Synthesis of Hierarchical ZSM-48 Nano-Zeolites. *New J. Chem.* **2018**, *42*, 4457−4464.

(21) Zhang, Y.; Ma, Y.; Che, S. Synthesis of Lamellar Mesostructured ZSM-48 Nanosheets. *Chem. Mater.* **2018**, *30*, 1839−1843.

(22) Zhang, M.; Li, C.; Chen, X.; Chen, Y.; Liang, C. Hierarchical ZSM-48-Supported Nickel Catalysts with Enhanced Hydroisomerization Performance of Hexadecane. *Ind. Eng. Chem. Res.* **2019**, *58*, 19855−19861.

(23) Kim, W.; Kim, J.-C.; Kim, J.; Seo, Y.; Ryoo, R. External Surface Catalytic Sites of Surfactant-Tailored Nanomorphic Zeolites for Benzene Isopropylation to Cumene. *ACS Catal.* **2013**, *3*, 192−195.

(24) Saenluang, K.; Srisuwanno, W.; Salakhum, S.; Rodaum, C.; Dugkhuntod, P.; Wattanakit, C. Nanoporous Sn-Substituted ZSM-48 Nanostructures for Glucose Isomerization. *ACS Appl. Nano Mater.* **2021**, *4*, 11661−11673.

(25) Zhang, M.; Wang, L.; Chen, Y.; Zhang, Q.; Liang, C. Creating Mesopores in ZSM-48 Zeolite by Alkali Treatment: Enhanced

Catalyst for Hydroisomerization of Hexadecane. *J. Energy Chem.* **2016**, *25*, 539−544.

(26) Zhou, J.; Liu, Z.; Li, L.; Wang, Y.; Gao, H.; Yang, W.; Xie, Z.; Tang, Y. Hierarchical Mesoporous ZSM-5 Zeolite with Increased External Surface Acid Sites and High Catalytic Performance in *o*-Xylene Isomerization. *Chin. J. Catal.* **2013**, *34*, 1429−1433.

(27) Wang, R.; Peng, Z.; Wu, P.; Sun, H.; Zhang, Y.; Subhan, F.; Yin, H.; Wang, Y.; Yan, Z. Direct synthesis of nanorod stacked "nest-like" hierarchical ZSM-48 hollow spheres using a triazine-based bolaform organic structure-directing agent. *Inorg. Chem. Front.* **2022**, *9*, 2016−2022.

(28) Tuel, A.; Farrusseng, D. Hollow Zeolite Single Crystals: Synthesis Routes and Functionalization Methods. *Small Methods* **2018**, *2*, 1800197.

(29) Chen, G. R.; Li, J. Y.; Wang, S.; Han, J.; Wang, X. X.; She, P. H.; Fan, W. B.; Guan, B. Y.; Tian, P.; Yu, J. H. Construction of Single-Crystalline Hierarchical ZSM-5 with Open Nanoarchitectures via Anisotropic-Kinetics Transformation for the Methanol-to-Hydrocarbons Reaction. *Angew. Chem., Int. Ed.* **2022**, *61*, No. e202200677.

(30) Dai, C.; Zhang, A.; Li, L.; Hou, K.; Ding, F.; Li, J.; Mu, D.; Song, C.; Liu, M.; Guo, X. Synthesis of Hollow Nanocubes and Macroporous Monoliths of Silicalite-1 by Alkaline Treatment. *Chem. Mater.* **2013**, *25*, 4197−4205.

(31) Zhai, Y.; Zhang, X.; Wang, F.; Lv, G.; Jiang, T.; Wu, Y.; Li, M.; Li, M.; Zhang, Q.; Liu, Y. Racing Crystallization Mechanism for Economical Design of Single-Crystal Hollow ZSM-5 with the Broken Limit of Si/Al Ratio and Improved Mass Transfer. *Appl. Mater. Interfaces* **2021**, *13*, 15246−15260.

(32) Zhao, D.; Wang, Y.; Chu, W.; Wang, X.; Zhu, X.; Li, X.; Xie, S.; Wang, H.; Liu, S.; Xu, L. Direct Synthesis of Hollow Single-Crystalline Zeolite Beta Using a Small Organic Lactam as a Recyclable Hollow-Directing Agent. *J. Mater. Chem. A* **2019**, *7*, 10795−10804.

(33) Morgado Prates, A. R.; Chetot, T.; Burel, L.; Pagis, C.; Martinez-Franco, R.; Dodin, M.; Farrusseng, D.; Tuel, A. Hollow Structures by Controlled Desilication of Beta Zeolite Nanocrystals. *J. Solid State Chem.* **2020**, *281*, 121033.

(34) Yuan, D.; Kang, C.; Wang, W.; Li, H.; Zhu, X.; Wang, Y.; Gao, X.; Wang, B.; Zhao, H.; Liu, C.; Shen, B. Creation of Mesostructured Hollow Y Zeolite by Selective Demetallation of An Artificial Heterogeneous Al Distributed Zeolite Crystal. *Catal. Sci. Technol.* **2016**, *6*, 8364−8374.

(35) Chu, N.; Wang, J.; Zhang, Y.; Yang, J.; Lu, J.; Yin, D. Nestlike Hollow Hierarchical MCM-22 Microspheres: Synthesis and Exceptional Catalytic Properties. *Chem. Mater.* **2010**, *22*, 2757−2763.

(36) Zhou, D.; Zhang, T.; Xia, Q.; Zhao, Y.; Lv, K.; Lu, X.; Nie, R. One-Pot Rota-Crystallized Hollownest-Structured Ti-zeolite: a Calcination-Free and Recyclable Catalytic Material. *Chem. Sci.* **2016**, *7*, 4966−4972.

(37) Li, J.; Liu, M.; Guo, X.; Xu, S.; Wei, Y.; Liu, Z.; Song, C. Interconnected Hierarchical ZSM-5 with Tunable Acidity Prepared by a Dealumination-Realumination Process: A Superior MTP Catalyst. *Appl. Mater. Interfaces* **2017**, *9*, 26096−26106.

(38) Al-Dughaither, A. S.; de Lasa, H. HZSM-5 Zeolites with Different SiO_2/Al_2O_3 Ratios. Characterization and NH_3 Desorption Kinetics. *Ind. Eng. Chem. Res.* **2014**, *53*, 15303−15316.

(39) Giordano, G.; Gabelica, Z.; Dewaele, N.; Nagy, J. B.; Derouane, E. G. Synthesis of Zeolite ZSM-48 with Different Organic and Inorganic Cations. *Stud. Surf. Sci. Catal.* **1991**, *60*, 29−36.

(40) Karwacki, L.; Stavitski, E.; Kox, M. H.; Kornatowski, J.; Weckhuysen, B. M. Intergrowth Structure of Zeolite Crystals as Determined by Optical and Fluorescence Microscopy of the Template-Removal Process. *Angew. Chem., Int. Ed.* **2007**, *46*, 7228−7231.

(41) Ikuno, T.; Chaikittisilp, W.; Liu, Z.; Iida, T.; Yanaba, Y.; Yoshikawa, T.; Kohara, S.; Wakihara, T.; Okubo, T. Structure-Directing Behaviors of Tetraethylammonium Cations toward Zeolite Beta Revealed by the Evolution of Aluminosilicate Species Formed during the Crystallization Process. *J. Am. Chem. Soc.* **2015**, *137*, 14533−14544.

https://doi.org/10.1021/acsami.2c16346